Progress in Flight Dynamics, GNC, and Avionics **6** (2013) 707-728
DOI: 10.1051/eucass/201306707

L_∞-OPTIMAL FEEDFORWARD GUST LOAD ALLEVIATION DESIGN FOR A LARGE BLENDED WING BODY AIRLINER

A. Wildschek[1], T. Haniš[2], and F. Stroscher[3]

[1]EADS Innovation Works
Munich 81663, Germany

[2]Czech Technical University in Prague
Prague 16627, Czech Republic

[3]Technische Universität München
Garching 85747, Germany

The potential advantages of Blended Wing Body (BWB) aircraft in terms of fuel efficiency are opposed by technical challenges such as the alleviation of gust loads. Due to the low wing, loading gusts, generally, have a more severe impact on BWB aircraft than on conventional aircraft. This paper presents the design and optimization of a Gust Load Alleviation System (GLAS) for a large BWB airliner. Numerical simulations are performed with an aeroelastic model of the aircraft including GLAS in order to compute time series of modal displacements for deriving equivalent static load cases which are used for the resizing of the aircraft structure.

1 INTRODUCTION

For a significant fuel efficiency improvement on long-range transport aircraft, the transition to BWB configurations offers a promising long-term solution. The advantage of higher lift-to-drag ratio is opposed by technical challenges such as the design of a flat pressurized cabin, specific demands on the control system due to the high coupling between flap deflections and aircraft movements in all three axes, handling asymmetric engine failure without tail as discussed in [1] as well as handling gust loads. Due to the low wing loading, BWB aircraft are generally more sensitive to gust loads than conventional wing tube aircraft. The investigations in this paper are based on the ACFA BWB (Active Control for Flexible BWB Aircraft), a 450-passenger configuration with two rear-mounted

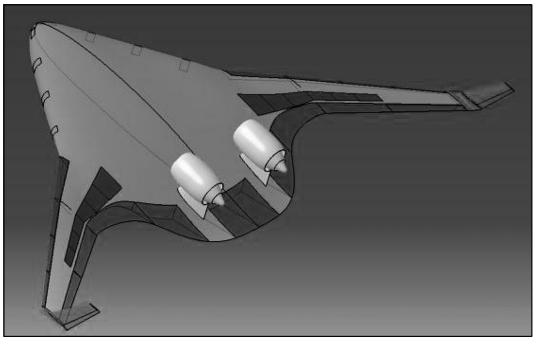

Figure 1 Control surface setting of the ACFA BWB

turbofan engines, which originates from the European project ACFA2020 (Active Control of Flexible 2020 Aircraft) (Fig. 1).

The structural concept is based on gust and manoeuver load computations. For some fuel configurations, the BWB airliner is statically unstable, thus requiring active stabilization. The coupled aeroelastic/flight mechanic BWB model used for this investigation is parameterized in Mach, dynamic pressure, fuel mass, and center of gravity (CG) position. Three discrete CG positions are considered. The CG variation is achieved by fuel redistribution which is important on a BWB airplane for trim without too large control surface deflections in order to achieve optimum cruise performance [2]. The other three model parameters are defined on a much finer grid.

In this investigation, the BWB airliner is controlled using 12 trailing edge flaps and 12 poilers on the upper side of the wings. Reasonable nonlinear actuators are modeled for actuation of said control surfaces. On each wing, three inner spoilers are actuated simultaneously and three outer spoilers are actuated simultaneously. Artificial pitch stiffness is basically achieved by feedback of the incremental vertical CG load factor Δn_z to 4 elevators. In order to achieve similar characteristics as for an aircraft with neutral stability, this feedback is done via a proportional-integral controller [3]. A pitch damper (i. e., feedback from pitch rate q to the elevators) allows placement of the poles of the angle of attack mode. In order to additionally damp the first symmetric wing bending mode, modal wing bending accelerations are measured for dynamic actuation of the outer wing trailing edge flaps [4]. The commands of the feedforward gust load alleviation system are just added to the commands of this flight control law. Taking into account manoeuvre load alleviation [5], gust loads become the dominant sizing factor. For efficient gust load alleviation, the weighted L_∞ norm of the responses of wing bending and torsion moment as well as shear force need to be minimized for gusts of different scale lengths throughout the whole flight

envelope while not exceeding maximum and minimum load factor. Section 2 will provide an optimization procedure for such GLAS considering these constraints.

2 GUST LOAD ALLEVIATION DESIGN

Lead time information about the gust is acquired at the aircraft nose by the alpha probe. The alpha probe measures $\alpha_{\text{air}}(t)$, a signal which contains a share due to gust as well as a share due to motion of the flexible aircraft. For the GLAS, however, $\alpha_{\text{wind}}(t)$ is required, i. e., only the share due to gust. According to [6], the computation of $\alpha_{\text{wind}}(t)$ is done by the following algorithm:

$$\alpha_{\text{wind}}(t) = \cos\left(\Phi(t)\right)\left[\arcsin\left(\frac{\dot{H}(t)}{V_{\text{TAS}}(t)}\right) - \Theta(t) + \cos\left(\Phi(t)\right)\left(\alpha_{\text{air}}(t) + \frac{q(t) r_{\text{AoA}}}{V_{\text{TAS}}(t)}\right) + \sin\left(\Phi(t)\right)\left(\beta - \frac{r(t) r_{\text{AoS}}}{V_{\text{TAS}}(t)}\right)\right]. \quad (1)$$

Thereby, $\Phi(t)$ is the bank angle in radians; $\dot{H}(t)$ is the aircraft's inertial vertical speed in m/s; $V_{\text{TAS}}(t)$ is the flight velocity of the aircraft in m/s with respect to the surrounding air; $\Theta(t)$ is the pitch angle in radians; $\beta(t)$ is the sideslip angle in radians; $r(t)$ is the yaw rate in rad/s; and r_{AoA} and r_{AoS} are the distances in meters from the CG to the alpha and to the beta sensor, respectively. Since, e. g., the vertical speed is computed by the inertia measurement unit by complementary filtering, this signal is delayed more than the other signals, which can be directly measured, such as the angle of attack of the alpha probe. In [6], it is suggested to artificially delay also the other signals; so, the equation for computation of alpha wind is mathematically correct. However, this introduces a delay on the reference signal required for feedforward gust load alleviation which is bad for reaction time of the GLAS. It was found that vertical speed does not need to be delayed because it changes very slowly anyhow. The GLAS control setup is similar to the one described in [7–9] and shown in Fig. 2 for the physical aircraft. Solid lines illustrate actual signals whereas dashed lines illustrate effects propagating through the atmosphere.

Exogenous disturbance in terms of (time dependent) vertical airflow stochastically distributed in space $w(t, x, y, z)$ excites the flexible aircraft. The share in the error signal vector $\vec{e}(t)$ coming from said disturbance is denoted disturbance signal vector $\vec{d}(t)$. Exogenous disturbance also excites the alpha probe which measures $\alpha_{\text{air}}(t)$. The signal $\alpha_{\text{wind}}(t)$ is high passed in order to get rid of constant components which cannot be accurately cancelled by Eq. (1). Resulting signal is shaped by Finite Impulse Response (FIR) filters with vector of transfer functions $\vec{H}(s)$ (i. e., one FIR filter per actuated control surface pair) in order to

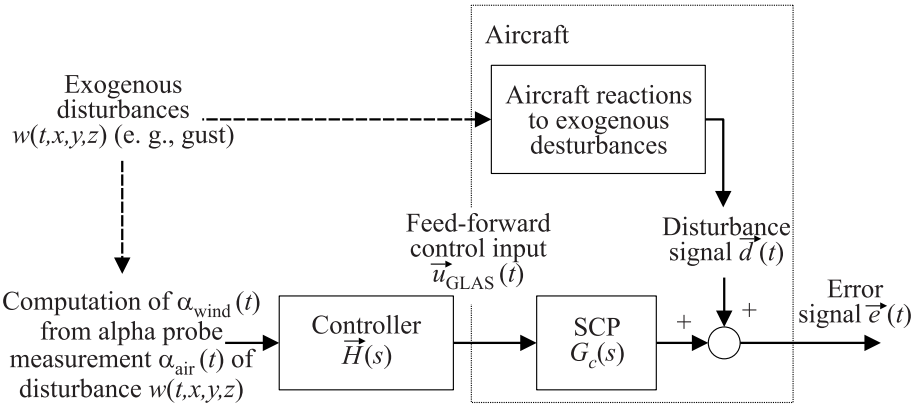

Figure 2 GLAS control setup

generate the control commands $\vec{u}_{\mathrm{GLAS}}(t)$ for different control surface pairs (e. g., symmetrically driven ailerons or spoilers or elevators). The effect of $\vec{u}_{\mathrm{GLAS}}(t)$ on $\vec{e}(t)$ is obtained by filtering $\vec{u}_{\mathrm{GLAS}}(t)$ by the so-called Secondary Control Path (SCP). Considering a mathematical model of the aircraft's equations of motion linearized in a certain trim point, the error signal $\vec{e}(t)$ is just the sum of $\vec{d}(t)$ and $\vec{u}_{\mathrm{GLAS}}(t)$, filtered by the matrix of transfer functions of the SCP, denoted $G_c(s)$. On the real aircraft, the error signal vector $\vec{e}(t)$ contains only physical signals (e. g., the incremental load factor $\Delta n_z(t)$) which can be used for in-flight monitoring of GLAS performance.

For GLAS optimization based on some model of the airplane, $\vec{e}(t)$ can also contain unphysical signals such as incremental wing bending and torsion moments as well as shear force at different wing cuts. The design objective is to adjust $\vec{H}(s)$ in order to minimize the L_∞-norm of a criteria based on forces and moments as will be explained later, keep $\Delta n_z(t)$ within certain limits (for passenger safety) and at the same time, do not exceed certain limits for the L_∞-norms of $\vec{u}_{\mathrm{GLAS}}(t)$, i. e., considering saturations of control surfaces. In this investigation, the GLAS uses 4 pairs of control surfaces: elevators, inner spoilers, outer spoilers, and symmetrically driven ailerons. The vector of control commands $\vec{u}_{\mathrm{GLAS}}(t)$ thus can be written as

$$\vec{u}_{\mathrm{GLAS}}(t) = \left(u_{\mathrm{el\,GLAS}}(t), u_{\mathrm{spoiler1\,GLAS}}(t), u_{\mathrm{spoiler2\,GLAS}}(t), u_{\mathrm{ai\,GLAS}}(t)\right)^{\mathrm{T}} .$$

The superscript T denotes transposition; $u_{\mathrm{el\,GLAS}}(t)$ denotes the GLAS command to elevators; $u_{\mathrm{spoiler1\,GLAS}}(t)$ denotes the GLAS command to the inner spoilers; $u_{\mathrm{spoiler2\,GLAS}}(t)$ denotes the GLAS command to the outer spoilers; and $u_{\mathrm{ai\,GLAS}}(t)$ denotes the GLAS command to ailerons. The discrete time control command for, e. g., elevators is generated by filtering a sampled version of high

passed signal $\alpha_{\text{wind}}(n)$ by an FIR filter with filter length N. Thus, in the following, all continuous time signals are used in discrete time with T_s denoting the sampling period, and n denoting the time step. With z denoting the z-transform variable and z^{-1}, therefore, denoting a one sample delay, the z-transfer function of the FIR controller for, e. g., the elevators $H_{\text{el}}(z)$ can be written as:

$$H_{\text{el}}(z) = h_{0\,\text{el}} + h_{1\,\text{el}} z^{-1} + h_{2\,\text{el}} z^{-2} + \cdots + h_{N-1\,\text{el}} z^{-N+1} \,.$$

The discrete time command to, e. g., the elevator at time step n is

$$u_{\text{el GLAS}}(n) = \vec{h}_{\text{el}}^{\,\text{T}} \vec{\alpha}(n) = \vec{\alpha}^{\,\text{T}}(n) \vec{h}_{\text{el}}$$

with

$$\vec{h}_{\text{el}} = [h_{0\,\text{el}},\ h_{1\,\text{el}},\ h_{2\,\text{el}},\ \ldots, h_{N-1\,\text{el}}]^{\text{T}}$$

denoting the vector of FIR coefficients, and $\vec{\alpha}(n)$ denoting the vector of the sampled reference signal at time step n:

$$\vec{\alpha}(n) = [\alpha(n),\ \alpha(n-1),\ \ldots, \alpha(n-N+1)]^{\text{T}} \,.$$

The discrete time signal $\alpha(n)$ is obtained by high pass filtering of $\alpha_{\text{wind}}(n)$ and feeding this signal through a threshold switch. Since in opposition to turbulence, a 1-cosine gust is a finite event of duration of $2H/V_{\text{TAS}}$, the discrete time sequence of $u_{\text{el GLAS}}(n)$ due to a gust measured by the alpha probe and after conditioning and sampling being fed through the FIR filter can be written as

$$\begin{pmatrix} \\ u_{\text{el GLAS}}(n=0) \\ u_{\text{el GLAS}}(n=1) \\ \cdots \\ u_{\text{el GLAS}}(n) \\ \cdots \\ u_{\text{el GLAS}}\left(n = F_s \dfrac{2H}{V_{\text{TAS}}} + N - 2\right) \\ u_{\text{el GLAS}}\left(n = F_s \dfrac{2H}{V_{\text{TAS}}} + N - 1\right) \\ 0 \\ \cdots \end{pmatrix}$$

$$= \begin{pmatrix} \alpha(n=0) & 0 & \cdots & 0 & 0 \\ \alpha(n=1) & \alpha(n=0) & \cdots & 0 & 0 \\ \cdots & \cdots & \cdots & \cdots & \cdots \\ \alpha(n) & \alpha(n-1) & \cdots & \alpha(n-N+2) & \alpha(n-N+1) \\ \cdots & \cdots & \cdots & \cdots & \cdots \\ 0 & 0 & \cdots & \alpha\left(n = F_s \frac{2H}{V_{\mathrm{TAS}}}\right) & \alpha\left(n = F_s \frac{2H}{V_{\mathrm{TAS}}} - 1\right) \\ 0 & 0 & \cdots & 0 & \alpha\left(n = F_s \frac{2H}{V_{\mathrm{TAS}}}\right) \\ 0 & 0 & \cdots & 0 & 0 \\ \cdots & \cdots & \cdots & \cdots & \cdots \end{pmatrix} \times \begin{pmatrix} h_{0\,\mathrm{el}} \\ h_{1\,\mathrm{el}} \\ \cdots \\ h_{N-2\,\mathrm{el}} \\ h_{N-1\,\mathrm{el}} \end{pmatrix}. \quad (2)$$

Here, H denotes the gust gradient distance and V_{TAS} is the true airspeed which is considered constant for the gust definition.

2.1 Formulation of the Optimization Problem

In the following, the constraints for optimization of the 4 FIR filters for control commands for elevators, inner spoilers, outer spoilers, and symmetrically driven ailerons are formulated. With sizing gusts of different lengths from 30 to 500 ft starting at time $t = 0$, it was sufficient to fulfill the following constraints within a time interval $[0; t_{\mathrm{end}}]$ of 10 s since oscillations excited by gust are diminished after that amount of time. On the one hand, the maximum and minimum control surface deflections need to be bounded by:

$$\left.\begin{aligned} u_{\mathrm{el\,GLAS}}(n) &\leq u_{\mathrm{el\,max}} \;\forall n \in [0; t_{\mathrm{end}} F_s]\,; \\ u_{\mathrm{el\,GLAS}}(n) &\geq u_{\mathrm{el\,min}} \;\forall n \in [0; t_{\mathrm{end}} F_s]\,; \end{aligned}\right\} \quad (3)$$

$$\left.\begin{aligned} u_{\mathrm{spoiler1\,GLAS}}(n) &\leq u_{\mathrm{spoiler1\,max}} \;\forall n \in [0; t_{\mathrm{end}} F_s]\,; \\ u_{\mathrm{spoiler1\,GLAS}}(n) &\geq u_{\mathrm{spoiler1\,min}} \;\forall n \in [0; t_{\mathrm{end}} F_s]\,; \\ u_{\mathrm{spoiler2\,GLAS}}(n) &\leq u_{\mathrm{spoiler2\,max}} \;\forall n \in [0; t_{\mathrm{end}} F_s]\,; \\ u_{\mathrm{spoiler2\,GLAS}}(n) &\geq u_{\mathrm{spoiler2\ min}} \;\forall n \in [0; t_{\mathrm{end}} F_s]\,; \\ u_{\mathrm{ai\,GLAS}}(n) &\leq u_{\mathrm{ai\ max}} \;\forall n \in [0; t_{\mathrm{end}} F_s]\,; \\ u_{\mathrm{ai\,GLAS}}(n) &\geq u_{\mathrm{ai\ min}} \;\forall n \in [0; t_{\mathrm{end}} F_s] \end{aligned}\right\} \quad (4)$$

with subscript 'max' denoting maximum allowed deflection of the respective control surface, and subscript 'min' denoting prescribed minimum allowed deflection of the respective control surface. On the other hand, the deflection rates $\dot{u}$ need to be limited because the available actuators' energy is finite. Thereby, F_s is the sampling frequency, and $T_s = 1/F_s$ denotes the sampling time of the discrete controller:

$$\left.\begin{aligned} \frac{u_{\mathrm{el\,GLAS}}(n) - u_{\mathrm{el\,GLAS}}(n-1)}{T_s} &\leq \dot{u}_{\mathrm{el\ max}} \ \forall n \in [1; t_{\mathrm{end}} F_s]\,; \\ \frac{u_{\mathrm{el\,GLAS}}(n) - u_{\mathrm{el\,GLAS}}(n-1)}{T_s} &\geq \dot{u}_{\mathrm{el\ min}} \ \forall n \in [1; t_{\mathrm{end}} F_s]\,; \end{aligned}\right\} \tag{5}$$

$$\left.\begin{aligned} \frac{u_{\mathrm{spoiler1\,GLAS}}(n) - u_{\mathrm{spoiler1\,GLAS}}(n-1)}{T_s} &\leq \dot{u}_{\mathrm{spoiler1\ max}} \ \forall n \in [1; t_{\mathrm{end}} F_s]\,; \\ \frac{u_{\mathrm{spoiler1\,GLAS}}(n) - u_{\mathrm{spoiler1\,GLAS}}(n-1)}{T_s} &\geq \dot{u}_{\mathrm{spoiler1\ min}} \ \forall n \in [1; t_{\mathrm{end}} F_s]\,; \\ \frac{u_{\mathrm{spoiler2\,GLAS}}(n) - u_{\mathrm{spoiler2\,GLAS}}(n-1)}{T_s} &\leq \dot{u}_{\mathrm{spoiler2\ max}} \ \forall n \in [1; t_{\mathrm{end}} F_s]\,; \\ \frac{u_{\mathrm{spoiler2\,GLAS}}(n) - u_{\mathrm{spoiler2\,GLAS}}(n-1)}{T_s} &\geq \dot{u}_{\mathrm{spoiler2\ min}} \ \forall n \in [1; t_{\mathrm{end}} F_s]\,; \\ \frac{u_{\mathrm{ai\,GLAS}}(n) - u_{\mathrm{ai\,GLAS}}(n-1)}{T_s} &\leq \dot{u}_{\mathrm{ai\ max}} \ \forall n \in [1; t_{\mathrm{end}} F_s]\,; \\ \frac{u_{\mathrm{ai\,GLAS}}(n) - u_{\mathrm{ai\,GLAS}}(n-1)}{T_s} &\geq \dot{u}_{\mathrm{ai\ min}} \ \forall n \in [1; t_{\mathrm{end}} F_s]\,. \end{aligned}\right\} \tag{6}$$

For passenger safety, the maximum and the minimum load factors need to be bounded too:

$$n_z(n) \leq 2.5 \ \ \forall n \in [0; t_{\mathrm{end}} F_s]\,; \quad n_z(n) \geq 0 \ \ \forall n \in [0; t_{\mathrm{end}} F_s]\,. \tag{7}$$

The cost function J is defined as a function of the vector of control commands $\vec{u}_{\mathrm{GLAS}}(n)$ with tuning paramters a_1, a_2, and a_3 and b_1, b_2, and b_3. Considering that positive as well as negative peak force and moment, the cost function J needs to be reduced for one sizing gust and one fuel case can be written as:

$$J = \max_n \Bigg[a_1 \Bigg(F_{z_0} + \sum_{i=0}^{t_{\mathrm{end}} F_s} f_{z_{\mathrm{Gust}}}(i) w(n-i) + \sum_{i=0}^{t_{\mathrm{end}} F_s} f_{z_{\mathrm{el}}}(i) u_{\mathrm{el\,GLAS}}(n-i) + \sum_{i=0}^{t_{\mathrm{end}} F_s} f_{z_{\mathrm{spoilers1}}}(i) u_{\mathrm{spoilers1\,GLAS}}(n-i)$$

$$+\sum_{i=0}^{t_{\text{end}}F_s} f_{z_{\text{spoilers2}}}(i)u_{\text{spoilers2 GLAS}}(n-i)+\sum_{i=0}^{t_{\text{end}}F_s} f_{z_{\text{ai}}}(i)u_{\text{ai GLAS}}(n-i)\Bigg)$$

$$+a_2\Bigg(M_{x_0}+\sum_{i=0}^{t_{\text{end}}F_s} m_{x_{\text{Gust}}}(i)w(n-i)+\sum_{i=0}^{t_{\text{end}}F_s} m_{x_{\text{el}}}(i)u_{\text{el GLAS}}(n-i)$$

$$+\sum_{i=0}^{t_{\text{end}}F_s} m_{x_{\text{spoilers1}}}(i)u_{\text{spoilers1 GLAS}}(n-i)$$

$$+\sum_{i=0}^{t_{\text{end}}F_s} m_{x_{\text{spoilers2}}}(i)u_{\text{spoilers2 GLAS}}(n-i)+\sum_{i=0}^{t_{\text{end}}F_s} m_{x_{\text{ai}}}(i)u_{\text{ai GLAS}}(n-i)\Bigg)$$

$$+a_3\Bigg(M_{y_0}+\sum_{i=0}^{t_{\text{end}}F_s} m_{y_{\text{Gust}}}(i)w(n-i)+\sum_{i=0}^{t_{\text{end}}F_s} m_{y_{\text{el}}}(i)u_{\text{el GLAS}}(n-i)$$

$$+\sum_{i=0}^{t_{\text{end}}F_s} m_{y_{\text{spoilers1}}}(i)u_{\text{spoilers1 GLAS}}(n-i)$$

$$+\sum_{i=0}^{t_{\text{end}}F_s} m_{y_{\text{spoilers2}}}(i)u_{\text{spoilers2 GLAS}}(n-i)+\sum_{i=0}^{t_{\text{end}}F_s} m_{y_{\text{ai}}}(i)u_{\text{ai GLAS}}(n-i)\Bigg)\Bigg]$$

$$-\min_n\Bigg[b_1\Bigg(F_{z_0}+\sum_{i=0}^{t_{\text{end}}F_s} f_{z_{\text{Gust}}}(i)w(n-i)+\sum_{i=0}^{t_{\text{end}}F_s} f_{z_{\text{el}}}(i)u_{\text{el GLAS}}(n-i)$$

$$+\sum_{i=0}^{t_{\text{end}}F_s} f_{z_{\text{spoilers1}}}(i)u_{\text{spoilers1 GLAS}}(n-i)$$

$$+\sum_{i=0}^{t_{\text{end}}F_s} f_{z_{\text{spoilers2}}}(i)u_{\text{spoilers2 GLAS}}(n-i)+\sum_{i=0}^{t_{\text{end}}F_s} f_{z_{\text{ai}}}(i)u_{\text{ai GLAS}}(n-i)\Bigg)$$

$$+b_2\Bigg(M_{x_0}+\sum_{i=0}^{t_{\text{end}}F_s} m_{x_{\text{Gust}}}(i)w(n-i)+\sum_{i=0}^{t_{\text{end}}F_s} m_{x_{\text{el}}}(i)u_{\text{el GLAS}}(n-i)$$

$$+\sum_{i=0}^{t_{\text{end}}F_s} m_{x_{\text{spoilers1}}}(i)u_{\text{spoilers1 GLAS}}(n-i)$$

$$+\sum_{i=0}^{t_{\text{end}}F_s} m_{x_{\text{spoilers2}}}(i)u_{\text{spoilers2 GLAS}}(n-i)+\sum_{i=0}^{t_{\text{end}}F_s} m_{x_{\text{ai}}}(i)u_{\text{ai GLAS}}(n-i)\Bigg)$$

$$+b_3\Bigg(M_{y_0}+\sum_{i=0}^{t_{\text{end}}F_s} m_{y_{\text{Gust}}}(i)w(n-i)+\sum_{i=0}^{t_{\text{end}}F_s} m_{y_{\text{el}}}(i)u_{\text{el GLAS}}(n-i)$$

$$+\sum_{i=0}^{t_{\text{end}}F_s} m_{y_{\text{spoilers1}}}(i)u_{\text{spoilers1 GLAS}}(n-i)$$
$$+\sum_{i=0}^{t_{\text{end}}F_s} m_{y_{\text{spoilers2}}}(i)u_{\text{spoilers2 GLAS}}(n-i)+\sum_{i=0}^{t_{\text{end}}F_s} m_{y_{\text{ai}}}(i)u_{\text{ai GLAS}}(n-i)\Bigg)\Bigg]. \quad (8)$$

For consideration of several sizing gusts and several fuel cases, Eq. (8) is extended by similar additional terms, which is not formulated here for the sake of clearness of this subsection. The GLAS is robustly optimized for several gust lengths between 30 and 500 ft and for 22 fuel configurations. Static shear force, torsion moment, and bending moment for $1g$ level flight are denoted F_{z_0}, M_{x_0}, and M_{y_0}; $w(n)$ is the discrete time gust excitation; and $f_{z_{\text{Gust}}}(i)$, $f_{z_{\text{el}}}(i)$, $f_{z_{\text{spoilers1}}}(i)$, $f_{z_{\text{spoilers2}}}(i)$, and $f_{z_{\text{ai}}}(i)$ denote the ith samples of shear force impulse responses of the linearized aircraft model to: gust excitation, elevators input, inner spoilers input, outer spoilers input, and ailerons input. At the same wing cut, respective impulse responses for torsion moment are denoted $m_{x_{\text{Gust}}}(i)$, $m_{x_{\text{el}}}(i)$, $m_{x_{\text{spoilers1}}}(i)$, $m_{x_{\text{spoilers2}}}(i)$, and $m_{x_{\text{ai}}}(i)$, and for bending moment $m_{y_{\text{Gust}}}(i)$, $m_{y_{\text{el}}}(i)$, $m_{y_{\text{spoilers1}}}(i)$, $m_{y_{\text{spoilers2}}}(i)$, and $m_{y_{\text{ai}}}(i)$. The optimization problem can thus be formulated as:

$$\min_{\vec{u}_{\text{GLAS}}} [J] \, . \quad (9)$$

Subject to: Eqs. (3)–(7).

2.2 Solution of the Optimization Problem

Numerical optimization was performed using linear longitudinal plant models for various fuel variants (with linear approximations of sensors and actuators) including phygoid, short period mode, 6 flexible modes and several lag states, and basic flight control system (FCS) [5] (Fig. 3).

For simplicity, the gusts are considered one-dimensional in this investigation, i. e., the exogenous disturbance $w(n)$ is still time dependent but not space dependent anymore. The interconnection of above aircraft model with the GLAS feedforward control is shown in Fig. 4.

The optimization problem defined by Eq. (9) can be reformulated as the following linear program (LP):

$$\begin{cases} \min\limits_{\vec{u}_{\text{GLAS}}} \vec{\gamma}\,; \\ A\vec{x} \le \vec{b}\,; \\ D\vec{u}_{\text{GLAS}}(n) \le \vec{c}\,. \end{cases} \quad (10)$$

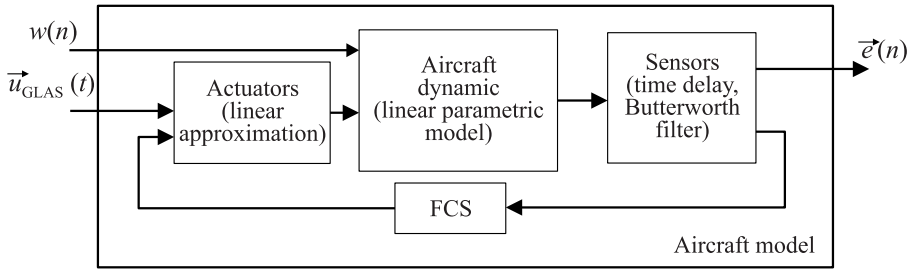

Figure 3 The GLAS design model

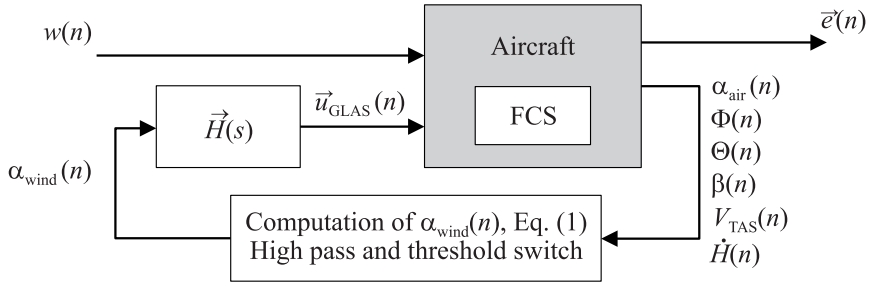

Figure 4 Feedforward control law interconnection

Here, according to Eq. (8), the objective function $\vec{\gamma}$ is defined by

$$\vec{\gamma} = [a_1,\ a_2,\ a_3,\ b_1,\ b_2,\ b_3] \cdot \begin{bmatrix} \gamma_1 \\ \gamma_2 \\ \gamma_3 \\ \gamma_4 \\ \gamma_5 \\ \gamma_6 \end{bmatrix} .$$

The decision variables $u_{\mathrm{GLAS}}(n)$ are the discrete time responses of the FIR controllers $H(z)$ to a measured 1-cosine gust, i. e., the left side of Eq. (2) extended to consider all 4 pairs of control surfaces. Note that in (10), the controller $\vec{H}(z)$ is implicitly contained in $\vec{u}_{\mathrm{GLAS}}(n)$. Therefore, the minimizer of the LP defined by (10) provides the L_∞ optimal control law. The optimization task is now defined as a linear program in a form directly suitable for some LMI parser which calls a linear solver.

In accordane with Eq. (8), in (10), the variable $\vec{x}$ is defined as

$$\vec{x} = \begin{bmatrix} 1 \\ u_{\text{el GLAS}}(0) \\ \vdots \\ u_{\text{el GLAS}}(N-1) \\ u_{\text{spoiler1 GLAS}}(0) \\ \vdots \\ u_{\text{spoiler1 GLAS}}(N-1) \\ u_{\text{spoiler2 GLAS}}(0) \\ \vdots \\ u_{\text{spoiler2 GLAS}}(N-1) \\ u_{\text{ai GLAS}}(0) \\ \vdots \\ u_{\text{ai GLAS}}(N-1) \end{bmatrix};$$

the variable $\vec{b}$ is defined as

$$\vec{b} = \begin{bmatrix} \left.\begin{matrix} 1 \\ \gamma_1 \cdot \vdots \\ 1 \end{matrix}\right\} t_{\text{end}} F_s \\ \left.\begin{matrix} 1 \\ \gamma_3 \cdot \vdots \\ 1 \end{matrix}\right\} t_{\text{end}} F_s \\ \left.\begin{matrix} 1 \\ 2.5 \cdot \vdots \\ 1 \end{matrix}\right\} t_{\text{end}} F_s \\ \left.\begin{matrix} 1 \\ -\gamma_4 \cdot \vdots \\ 1 \end{matrix}\right\} t_{\text{end}} F_s \\ \left.\begin{matrix} 1 \\ -\gamma_6 \cdot \vdots \\ 1 \end{matrix}\right\} t_{\text{end}} F_s \\ \left.\begin{matrix} 1 \\ 0 \cdot \vdots \\ 1 \end{matrix}\right\} t_{\text{end}} F_s \end{bmatrix}; \tag{11}$$

and the variable A is defined as

$$A = \begin{bmatrix} A_1 \\ -A_1 \end{bmatrix}$$

where

$$A_1 = \begin{bmatrix}
F_{z_0} + f_{z_{\mathrm{Gust}(0)}} & f_{z_{\mathrm{el}(0)}} & 0 & \cdots \\
\vdots & \vdots & f_{z_{\mathrm{el}(0)}} & \cdots \\
\vdots & \vdots & \vdots & \cdots \\
\vdots & \vdots & \vdots & \cdots \\
\vdots & \vdots & \vdots & \cdots \\
F_{z_0} + f_{z_{\mathrm{Gust}(t_{\mathrm{end}\,F_s})}} & f_{z_{\mathrm{el}(t_{\mathrm{end}\,F_s})}} & f_{z_{\mathrm{el}(t_{\mathrm{end}\,F_s}-1)}} & \cdots \\
M_{x_0} + m_{x_{\mathrm{Gust}(0)}} & m_{x_{\mathrm{el}(0)}} & 0 & \cdots \\
\vdots & \vdots & m_{x_{\mathrm{el}(0)}} & \cdots \\
\vdots & \vdots & \vdots & \cdots \\
\vdots & \vdots & \vdots & \cdots \\
\vdots & \vdots & \vdots & \cdots \\
M_{x_0} + m_{x_{\mathrm{Gust}(t_{\mathrm{end}\,F_s})}} & m_{x_{\mathrm{el}(t_{\mathrm{end}\,F_s})}} & m_{x_{\mathrm{el}(t_{\mathrm{end}\,F_s}-1)}} & \cdots \\
M_{y_0} + m_{y_{\mathrm{Gust}(0)}} & m_{y_{\mathrm{el}(0)}} & 0 & \cdots \\
\vdots & \vdots & m_{y_{\mathrm{el}(0)}} & \cdots \\
\vdots & \vdots & \vdots & \cdots \\
\vdots & \vdots & \vdots & \cdots \\
\vdots & \vdots & \vdots & \cdots \\
M_{y_0} + m_{y_{\mathrm{Gust}(t_{\mathrm{end}\,F_s})}} & m_{y_{\mathrm{el}(t_{\mathrm{end}\,F_s})}} & m_{y_{\mathrm{el}(t_{\mathrm{end}\,F_s}-1)}} & \cdots \\
n_{z_{\mathrm{Gust}(0)}} & n_{z_{\mathrm{el}(0)}} & 0 & \cdots \\
\vdots & \vdots & n_{z_{\mathrm{el}(0)}} & \vdots \\
\vdots & \vdots & \vdots & \cdots \\
\vdots & \vdots & \vdots & \cdots \\
\vdots & \vdots & \vdots & \cdots \\
n_{z_{\mathrm{Gust}(t_{\mathrm{end}\,F_s})}} & n_{z_{\mathrm{el}(t_{\mathrm{end}\,F_s})}} & n_{z_{\mathrm{el}(t_{\mathrm{end}\,F_s}-1)}} & \cdots
\end{bmatrix}$$

$$
\begin{bmatrix}
\cdots & 0 & \cdots & f_{z_{\mathrm{ai}(0)}} & \cdots & 0 \\
\cdots & \vdots & \cdots & \vdots & \cdots & \vdots \\
\cdots & 0 & \cdots & \vdots & \cdots & 0 \\
\cdots & f_{z_{\mathrm{el}(0)}} & \cdots & \vdots & \cdots & f_{z_{\mathrm{ai}(0)}} \\
\cdots & \vdots & \cdots & \vdots & \cdots & \vdots \\
\cdots & f_{z_{\mathrm{el}(t_{\mathrm{end}}F_s-N)}} & \cdots & f_{z_{\mathrm{ai}(t_{\mathrm{end}}F_s)}} & \cdots & f_{z_{\mathrm{el}(t_{\mathrm{end}}F_s-N)}} \\
\cdots & 0 & \cdots & m_{x_{\mathrm{ai}(0)}} & \cdots & 0 \\
\cdots & \vdots & \cdots & \vdots & \cdots & \vdots \\
\cdots & 0 & \cdots & \vdots & \cdots & 0 \\
\cdot & m_{x_{\mathrm{el}(0)}} & \cdots & \vdots & \cdots & m_{x_{\mathrm{ai}(0)}} \\
\cdots & \vdots & \cdots & \vdots & \cdots & \vdots \\
\cdots & m_{x_{\mathrm{el}(t_{\mathrm{end}}F_s-N)}} & \cdots & m_{x_{\mathrm{ai}(t_{\mathrm{end}}F_s)}} & \cdots & m_{x_{\mathrm{ai}(t_{\mathrm{end}}F_s-N)}} \\
\cdots & 0 & \cdots & m_{y_{\mathrm{ai}(0)}} & \cdots & 0 \\
\cdots & \vdots & \cdots & \vdots & \cdots & \vdots \\
\cdots & 0 & \cdots & \vdots & \cdots & 0 \\
\cdots & m_{y_{\mathrm{el}(0)}} & \cdots & \vdots & \cdots & m_{y_{\mathrm{ai}(0)}} \\
\cdots & \vdots & \cdots & \vdots & \cdots & \vdots \\
\cdots & m_{y_{\mathrm{el}(t_{\mathrm{end}}F_s-N)}} & \cdots & m_{y_{\mathrm{ai}(t_{\mathrm{end}}F_s)}} & \cdots & m_{y_{\mathrm{ai}(t_{\mathrm{end}}F_s-N)}} \\
\cdots & 0 & \cdots & n_{z_{\mathrm{ai}(0)}} & \cdots & 0 \\
\vdots & \vdots & \vdots & \vdots & \cdots & \vdots \\
\cdots & 0 & \cdots & \vdots & \cdots & 0 \\
\cdots & n_{z_{\mathrm{el}(0)}} & \cdots & \vdots & \cdots & n_{z_{\mathrm{ai}(0)}} \\
\cdots & \vdots & \cdots & \vdots & \cdots & \vdots \\
\cdots & n_{z_{\mathrm{el}(t_{\mathrm{end}}F_s-N)}} & \cdots & n_{z_{\mathrm{ai}(t_{\mathrm{end}}F_s)}} & \cdots & n_{z_{\mathrm{ai}(t_{\mathrm{end}}F_s-N)}}
\end{bmatrix} ; \tag{12}
$$

The computational effort with respect to memory demands can grow really fast, as it is a function of the number of variables, i. e., the number of used control surfaces, the time horizon of optimization, the time horizon of control, the number of considered operation points, and the sampling period. Thus, one option for the reduction of said memory burden is to evaluate the criterion in sparse points only, iteratively adding points whenever constrains are violated.

Note that the constraint in Eq. (7) is considered in Eqs. (11) and (12). In accordance with Eqs. (3)–(6), the D variable is defined as

$$D = \begin{bmatrix} D_1 \\ -D_1 \\ D_2 \\ -D_2 \end{bmatrix} \; ; \quad D_1 = \begin{bmatrix} I_{N\times N} & 0 & 0 & 0 \\ 0 & I_{N\times N} & 0 & 0 \\ 0 & 0 & I_{N\times N} & 0 \\ 0 & 0 & 0 & I_{N\times N} \end{bmatrix} \; ; \quad D_2 = \begin{bmatrix} I_D & 0 & 0 & 0 \\ 0 & I_D & 0 & 0 \\ 0 & 0 & I_D & 0 \\ 0 & 0 & 0 & I_D \end{bmatrix}$$

where the finite differences for approximation of the discrete derivative in Eqs. (5) and (6) are contained in:

$$I_D = \begin{bmatrix} -1 & 1 & 0 & \cdots & 0 \\ 0 & \ddots & \ddots & \ddots & \vdots \\ \vdots & \ddots & \ddots & \ddots & 0 \\ 0 & \cdots & 0 & -1 & 1 \end{bmatrix}_{(N-1)\times N} .$$

The variable $\vec{c}$ is defined as $\vec{c} = \begin{bmatrix} \vec{c}_1 \\ \vec{c}_2 \end{bmatrix}$ where $\vec{c}_1$ is determined in accordance with Eqs. (3) and (4) and $\vec{c}_2$ in accordance with Eqs. (5) and (6):

$$\vec{c}_1 = \begin{bmatrix} u_{\text{el max}} \cdot \underbrace{\begin{matrix} 1 \\ \vdots \\ 1 \end{matrix}}_{N} \\ u_{\text{spoiler1 max}} \cdot \underbrace{\begin{matrix} 1 \\ \vdots \\ 1 \end{matrix}}_{N} \\ u_{\text{spoiler2 max}} \cdot \underbrace{\begin{matrix} 1 \\ \vdots \\ 1 \end{matrix}}_{N} \\ u_{\text{ai max}} \cdot \underbrace{\begin{matrix} 1 \\ \vdots \\ 1 \end{matrix}}_{N} \\ u_{\text{el min}} \cdot \underbrace{\begin{matrix} 1 \\ \vdots \\ 1 \end{matrix}}_{N} \\ u_{\text{spoiler1 min}} \cdot \underbrace{\begin{matrix} 1 \\ \vdots \\ 1 \end{matrix}}_{N} \\ u_{\text{spoiler2 min}} \cdot \underbrace{\begin{matrix} 1 \\ \vdots \\ 1 \end{matrix}}_{N} \\ u_{\text{ai min}} \cdot \underbrace{\begin{matrix} 1 \\ \vdots \\ 1 \end{matrix}}_{N} \end{bmatrix} \; ; \quad \vec{c}_2 = \begin{bmatrix} T_s \dot{u}_{\text{el max}} \cdot \underbrace{\begin{matrix} 1 \\ \vdots \\ 1 \end{matrix}}_{N-1} \\ T_s \dot{u}_{\text{spoiler1 max}} \cdot \underbrace{\begin{matrix} 1 \\ \vdots \\ 1 \end{matrix}}_{N-1} \\ T_s \dot{u}_{\text{spoiler2 max}} \cdot \underbrace{\begin{matrix} 1 \\ \vdots \\ 1 \end{matrix}}_{N-1} \\ T_s \dot{u}_{\text{ai max}} \cdot \underbrace{\begin{matrix} 1 \\ \vdots \\ 1 \end{matrix}}_{N-1} \\ T_s \dot{u}_{\text{el min}} \cdot \underbrace{\begin{matrix} 1 \\ \vdots \\ 1 \end{matrix}}_{N-1} \\ T_s \dot{u}_{\text{spoiler1 min}} \cdot \underbrace{\begin{matrix} 1 \\ \vdots \\ 1 \end{matrix}}_{N-1} \\ T_s \dot{u}_{\text{spoiler2 min}} \cdot \underbrace{\begin{matrix} 1 \\ \vdots \\ 1 \end{matrix}}_{N-1} \\ T_s \dot{u}_{\text{ai min}} \cdot \underbrace{\begin{matrix} 1 \\ \vdots \\ 1 \end{matrix}}_{N-1} \end{bmatrix} .$$

2.3 Results of Numeric Optimization

As expected, the most restrictive constraint is Eq. (16) since due to the low wing loading, sizing updraft gusts can cause vertical load factors of $3g$ and more on the ACFA BWB aircraft (Fig. 5). Unless elevator constraints as defined by Eqs. (3) and (5) are set to unrealistically high values, no solution was found for $\vec{u}_{\mathrm{GLAS}}(n)$ which would fulfill Eq. (7). The reduction of load factor was only possible by rapid elevator deflection which pitches the aircraft into the gust. Deflection of spoilers is shown to be an efficient measure for reduction of wing loads, but causes a high pitch-up moment which in fact increases the angle of attack and, thus, the vertical load factor. This behavior is mainly due to the fact that the ACFA BWB is a high wing configuration and, thus, the spoilers drag force has a high lever arm with respect to the CG. Figure 5 illustrates total bending moment $M_x(n)$ (i. e., multiplier of a_3 in Eq. (8)) at a representative wing cut (Fig. 5*a*) and vertical acceleration at CG $N_z(n)$ (Fig. 5*b*) for 11 fuel cases resulting from an optimization run with relaxed constraints on rate limitation

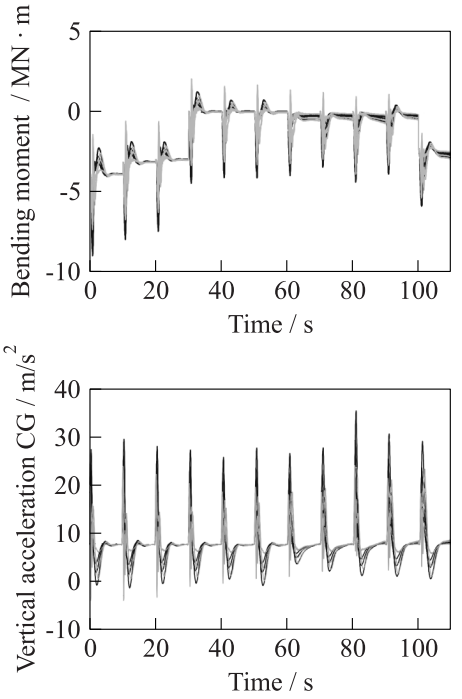

Figure 5 Responses of $M_x(n)$ and $N_z(n)$ with relaxed constraints on elevators' rate limit (black — without GLAS; and grey — with GLAS)

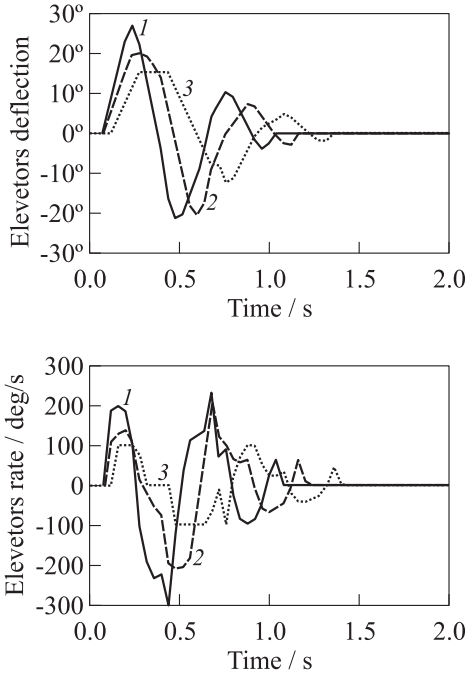

Figure 6 Required elevators' deflection $u_{\text{el GLAS}}(n)$ and respective rate for three different sizing gusts: *1* — elevators response to a sizing 250-feet gust; *2* — 350-feet gust; and *3* — elevators response to a sizing 500-feet gust

for $u_{\text{el GLAS}}(n)$ for maximum operating Mach number at an altitude of 28,743 ft. The responses for each of the 11 fuel cases are consecutively plotted for 10 s resulting in overall 110 s for the X-axis. The results for three different gust gradient distances H are plotted on top of each other. It can be seen that the maximum bending moment is reduced by almost 20% while constraints on $N_z(n)$ are fulfilled.

As illustrated by Fig. 6, the elevators' deflection $u_{\text{el GLAS}}(n)$ was limited to $\pm 15^\circ$ and the respective rate was at least limited to ± 10 deg/s for encounter of a 500-feet sizing gust (*3*). For smaller gust gradient distances the resulting deflections and rates are accordingly higher due to the frequency content of the excitation. Note that loads and load factor due to the 500-feet gust are much higher than for the 250- and 350-feet gust. Thus, the huge deflections and deflection rates resulting for the 250- and 350-feet gust can be neglected for the following discussion, since they are just a result of the GLAS control law being aggressively optimized for the 500-feet gust. Since the deflections required to satisfy Eq. (7) are fairly large even for the 500-feet gust, a reduction

of elevators' size would not be a reasonable means for increasing the elevators' bandwidth using the same actuators. Actuators that would be able to deflect the huge elevators of the ACFA BWB at the rates of 100 deg/s and more are most probably too heavy and too energy-consuming for efficient use on a commercial transport aircraft.

3 NUMERIC SIMULATIONS OF THE GUST LOAD ALLEVIATION SYSTEM

Numeric simulations with and without GLAS are performed with a flexible aircraft model linearized at various representative trim points. The simulation model includes nonlinear forth-order actuators for the trailing edge control surfaces and spoilers, sensor delays, and flight control laws. Encounter of sizing gusts of different gust gradient distances are simulated in accordance with Federal Aviation Regulations [10]. Figure 7 illustrates $M_x(t)$ and $N_z(t)$ resulting from simulations at maximum operating Mach number and altitudes ranging

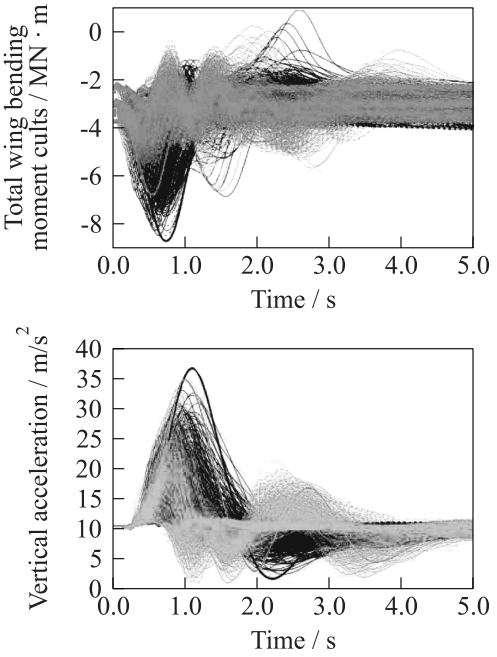

Figure 7 Simulated $M_x(t)$ and $N_z(t)$ for sizing gust encounters considering nonlinear actuator models (black — without GLAS; and grey — with GLAS)

from 28,743 to 38,638 ft. The GLAS used in this simulation was designed robust with respect to different fuel cases and gust gradient distances considering reasonable constraints for maximum elevators' deflection rates. The total bending moment is still reduced by 20%. The vertical acceleration $N_z(t)$, however, cannot be reduced using the nonlinear actuators, i. e., considering limitations on available actuators' energy.

4 STRUCTURAL RESIZING OF THE BLENDED WING BODY AIRCRAFT

The impact of load alleviation on fuel efficiency may reasonably be assessed by means of potential structural weight savings. A complete balance of additional weight, required by the load alleviation system, as well as weight savings with regards to the load bearing structure may lead to a conclusion in the early concept phase. The latter will be identified by resizing in terms of structural optimization. In a first design step, the structural optimization routine is applied to achieve a structural design considering sizing gusts and manoeuvres without active load alleviation. This design serves as a reference for the assessment of load alleviation performance. The second design step provides a structural design fulfilling the same requirements as the reference, but best possibly exploiting the control concepts for active load alleviation.

4.1 Model Setup

The structural optimization routine employs the finite-element model of the BWB aircraft, which has been applied in aeroelastic modelling before. All load bearing parts of the wing structure are assigned to design regions distributed over the wingspan (Fig. 8*a*).

The stringer stiffened skin is represented by composite elements with smeared stringers. The stiffness and mass properties of the panels are computed from design variables for stringer thickness t_{str} and skin thickness t_{sk} for each design zone, as shown in Fig. 8*b*. For structural optimization, the gradient-based solver MSC Nastran SOL200 [11] is applied. The objective of the optimization task is the minimization of overall mass. Constraints are applied for composite strains, as well as for analytic buckling criteria for the skin panels. In initial structural design of the wing, flutter speed was a critical design driver. Thus, a flutter speed check is implemented as constraint, as this value is influenced by the wingbox structural design.

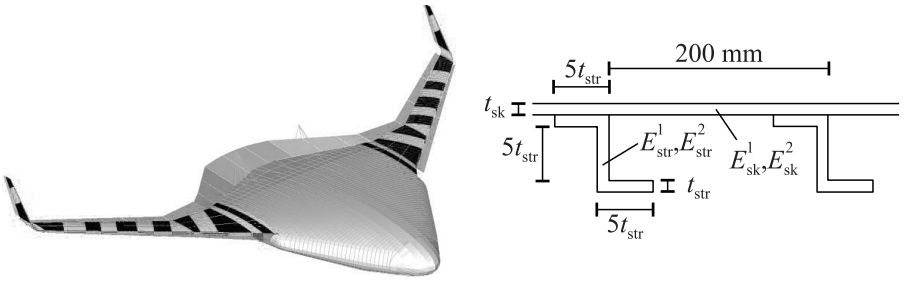

Figure 8 Design regions of the BWB wing (a) and stringer/panel design variables (b)

4.2 Load Cases

All load scenarios to be applied in structural resizing are derived from results of time-domain simulations of the BWB model. Longitudinal and lateral transient manoeuvres as well as discrete gust loads are considered. The so-called Mode Displacement Method (MDM) [12] is applied here for deriving equivalent static load cases from the modal displacement time histories η_e derived from numeric simulations of, e. g., gust encounter as described in section 3. With known modal matrix Φ_{ge} and stiffness matrix K_{gg} of same finite-element model applied in aeroelastic modeling, equivalent static load cases can be computed by

$$\left\{ \begin{array}{c} \{F\}_i \\ \{M\}_i \end{array} \right\} = [K_{gg}]\,[\Phi_{ge}]\,\{\eta_e\}\,.$$

The MDM leads to a very large number of load cases, if applied for all time steps in simulation. However, the MSC Nastran SOL200 solver is programmed to automatically identify critical load cases for further consideration in the following optimization cycles. This method dramatically reduces the computational costs and makes the analysis of manifold loadcases feasible. Further, critical timesteps to be applied for loads analysis, are identified from simulation history via bending moments and displacement signals.

4.3 Structural Optimization

The optimization problem is formulated as mass minimization with afore mentioned design variables and constraints. The optimization results are shown in terms of wing panel and stringer thicknesses of the design zones over wing span in Fig. 9. Figure 9a shows the resulting thicknesses for structural optimization without load alleviation, whereas Fig. 9b shows the results for the design

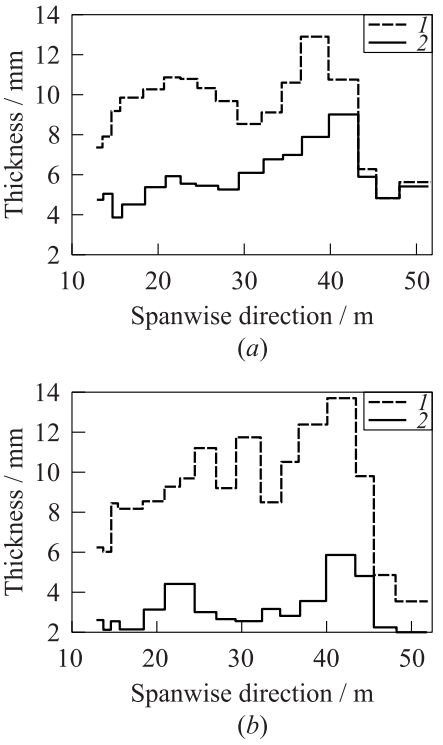

Figure 9 Optimized thicknesses of panels (*1*) and stringers (*2*) over wingspan (including winglet span)

with load alleviation considered. Independently from load alleviation, it can be seen that the outboard panels and stringers are remarkably reinforced by the optimization program. By observation of the active flutter constraint and its sensitivities, it was concluded that the outboard thickness increase is the most effective measure for flutter prevention, considering given optimization problem. The main effect of load alleviation on structural design is that the stringer thickness over the whole wing span can be decreased significantly. The total mass saving of the full aircraft due to load alleviation was found to be about 2 metric tons, or 0.5% of the aircraft's maximum take-off weight.

5 CONCLUDING REMARKS

This paper presents the design and optimization of a GLAS for a large BWB airliner. Structural loads are shown to be effectively reduced by the GLAS with

the available actuators which allows for a resizing of the aircraft's wing structure resulting in significant mass savings. Buckling as well as flutter constraints are considered in the structural optimization. Vertical accelerations during gust encounter, however, are huge and cannot be reduced unless much more powerful actuators are provided for the elevators in order to be able to rapidly pitch the BWB aircraft into a gust and, thus, reduce the additional angle of attack. However, size, mass, and power consumption of such actuators is most probably too large for reasonable use on an efficiency-driven aircraft design. Future research should, thus, be dedicated to investigating other unconventional devices which can pitch the BWB aircraft into a gust using less control power. Another field of research is considering GLAS certification requirements in the optimization process for overall aircraft mass minimization.

ACKNOWLEDGMENTS

The authors would like to thank the European Commission for funding the ACFA2020 project within the 7th Research Framework Programme as well as all ACFA2020 partners.

REFERENCES

1. Wildschek, A., T. Havar, and K. Plötner. 2009. An all-composite, all-electric, morphing trailing edge device for flight control on a blended-wing-body airliner. *Proc. IMechE, Part G: J. Aerospace Eng.* 224(G1):1–9.
2. Wildschek, A., F. Stroscher, T. Haniš, and T. Belschner. 2013. Fuel management system for cruise performance optimization on a large blended wing body airliner. In: *Progress in flight dynamics, guidance, navigation, control, fault detection, and avionics*. Eds. Ch. Vallet, D. Choukroun, Ch. Philippe, G. Balas, A. Nebylov, and O. Yanova. EUCASS advances in aerospace sciences book ser. Moscow: TORUS PRESS. 6:651–70.
3. Brockhaus, R. 2001. *Flugregelung. 2. Auflage*. Berlin: Springer. 655–59.
4. Wildschek, A., F. Stroscher, T. H. Klimmek, Z. Šika, T. Vampola, M. Valášek, D. Gangsaas, N. Aversa, and A. Berard. 2010. Gust load alleviation on a large blended wing body airliner. *ICAS2010 — 27th Congress of the International Council of the Aeronautical Sciences*. Nice, France.
5. Westermayer, C., A. Schirrer, M. Hemedi, and M. Kozek. 2013. An $\mathcal{H}_\infty$ full information approach for the feedforward controller design of a large blended wing body flexible aircraft. In: *Progress in flight dynamics, guidance, navigation, control, fault detection, and avionics*. Eds. Ch. Vallet, D. Choukroun, Ch. Philippe, G. Balas, A. Nebylov, and O. Yanova. EUCASS advances in aerospace sciences book ser. Moscow: TORUS PRESS. 6:685–706.

6. Hahn, K.-U. 2007. Apparatus and method for reducing the impact of turbulence and gusts on aircraft. European Patent EP 1 854 717 A1.
7. Wildschek, A., R. Maier, F. Hoffmann, M. Jeanneau, and N. Aversa. 2009. Minimizing dynamic structural loads of an aircraft. U.S. Patent US 2009/0084908.
8. Wildschek, A. 2009. An adaptive feed-forward controller for active wing bending vibration alleviation on large transport aircraft. Dissertation. München: Technische Universität.
9. Wildschek A., R. Maier, K.-U. Hahn, D. Leißling, M. Preß, and A. Zach. 2009. Flight test with an adaptive feed-forward controller for alleviation of turbulence excited wing bending vibrations. *AIAA Guidance, Navigation, and Control Conference and Exhibit*. Chicago, IL.
10. Federal Aviation Regulations. 1980. Part 25 — Airworthiness standards: Transport category airplanes. U.S. Department of Transportation, Federal Aviation Administration. Also: Code of Federal Regulations, title 14, aeronautics and space, Part 25 — Airworthiness standards: Transport category airplanes.
11. 2010. MD/MSC Nastran 2010 Design Sensitivity and Optimization User's Guide. MSC.Software Corporation.
12. Kier, T., and G. Looye. 2009. Unifying manoeuvre and gust loads analysis models. *Forum (International) of Aeroelasticity and Structural Dynamics*.